https://doi.org/10.62836/iaet.v2i1.201

Global Science Publishing

IAET

Innovations in Applied Engineering and Technology

https://ojs.sgsci.org/journals/iaet

Article

Performance Enhancement of AlGaN-based Deep Ultraviolet Light-emitting Diodes with $Al_xGa_{1-x}N$ Linear Descending Layers

Xiaoyang Chen [1] and Huitao Zhang [2,*]

[1] *Radiawave Co., Ltd., Shen Zhen, China; chenxiaoyang@radiawave.com*

[2] *Northen Arizona University, Flagstaff, AZ 86011, USA*

Abstract: In this work, the optical performance of AlGaN-based deep ultraviolet light-emitting diode (DUV LED) with $Al_xGa_{1-x}N$ linear descending layers has been investigated. The calculated results indicate that the novel DUV LED has better internal quantum efficiency and higher light output power compared with conventional DUV LED. These improvements are attributed to the design of $Al_xGa_{1-x}N$ linear descending layers, including n-type layer (NTL), linear Al-composition graded (LACG) quantum barriers (QBs) and hole suply layer (HSL), which induces more electrons and holes to flow into the active region, and decreases the electron leakage, thus improving the carrier concentrations in the quantum wells (QWs) and enhancing the radiation recombination rate of LED.

Keywords: DUV LED; $Al_xGa_{1-x}N$; linear descending layers; internal quantum efficiency

1. Introduction

Ultraviolet light of less than 300 nm has the antiviral effects on bacteria and viruses, and AlGaN-based ultraviolet light-emitting diode (DUV LED) has been demonstrated recently that it's effective to inactivate the coronavirus disease of 2019 (COVID-19), which is caused by the novel coronavirus SARS-CoV-2 [1 – 3]. Additionally, these DUV LEDs also exhibit continuous frequency tunability in terahertz bio-sensing and spectroscopy [4]. Besides sterilization, AlGaN-based DUV LED has also been widely employed in water purification, high-density optical memory, biochemistry and photolithography, which has attracted much attention due to its energy-efficiency performance. However, the internal quantum efficiency (IQE) of DUV LED is still very lower and restricts the large-scale commercial use. Improving IQE is a research focus of DUV LED, and it is primarily dependent on the crystal quality, the LED structure and the available number of carriers in the multiple quantum wells (MQWs) for the radiative recombination. At present, many solutions have been proposed [3, 5], such as decreasing the electron leakage, increasing the hole injection, modulating polarized electronstatic field [6,7]. To this end, a variety of DUV LED structures are designed. For example, introducing novel electron blocking layer (EBL): superlattice EBL [7,8], undoped BAlN EBL [9], double side graded EBL [10], w-shaped EBL [11], p-AlInN EBL [12] and so on. A highly transmissive helical terahertz plasmonic antenna proposed by Deng et al. can be utilized to optimize LED design [13]. Their later research further demonstrates that integrating surface plasmonic graphene technology enables multi-frequency resonant

Received: 28 September 2023; Accepted: 23 October 2023.

* Corresponding: Huitao Zhang (hz345@nau.edu)

photodetection in the mid-infrared range, thereby expanding the application of LEDs in optoelectronic detection [14]. Altering LED structure: ultrathin GaN/AlN MQW [15], grading quantum barriers [16], hole injection layer [17, 18], stepped and superlattice n-type confinement layer [19]. It's noteworthy that the higher polarization field in the active region of AlGaN LED is related to high quantum confined stark effect (QCSE) [20], which reduces the radiactive recombination rate and causes the redshift of luminous peak, so it's critical to reduce the QCSE in MQWs. Some related studies, including the partially-graded quantum barrier (QB) and quantum well in AlGaN DUV LEDs, have been done to reduce the QCSE [6, 7, 21, 22]. Additionally, recent research has demonstrated the application of machine learning in system reliability analysis, providing new insights for optimizing LED design. Machine learning can enhance overall LED performance through performance optimization and prediction, material property analysis, defect detection and quality control, optical property modeling, thermal management, and automated design and optimization [23–25].

Recently, Zhang *et al.* used p+-GaN/$In_{0.15}Ga_{0.85}N$/n+-GaN tunnel junction on DUV LED to enhance the hole injection [26]. Sharif *et al.* reported that $Al_{0.96}In_{0.04}N/Al_{0.98}In_{0.02}N$ superlattice EBL can help to develop a more efficient AlGaN DUV LED [12]. The researches have shed light on a proper structural design for high-efficiency DUV LED. Sugaya and Deng also indicated that tuning the resonant frequency of terahertz plasmonic structures could further improve the efficiency of DUV LEDs [27]. Here, we focus on optimized LED structure with $Al_xGa_{1-x}N$ linear descending layers, which shows some inspiring results, such as less electron overflow, more hole injection and a lower electronstatic field in MQWs,these bring higher radiative recombination.

2. Structures and Method

The structural diagrams of four DUV LEDs are shown in Figure 1. The c-plane sapphire substrate and AlN/$Al_{0.55}G_{0.45}N$ superlattice buffer layer are used, LED chip size is set to be 300 μm×300 μm. For comparison, a conventional DUV-LED structure is introduced and denoted as S0, it is constructed with a 3 μm-thick Si-doped $Al_{0.55}Ga_{0.45}N$(n-type concentration of 5×10^{18} cm^{-3}), 10nm-thick Si-doped $Al_{0.6}Ga_{0.4}N$ layer (n-type concentration of 5×10^{18} cm^{-3}), active region, 10 nm-thick Mg-doped $Al_{0.6}Ga_{0.4}N$ EBL (p-type concentration of 1×10^{18} cm^{-3}), 10nm-thick Mg-doped $Al_{0.55}Ga_{0.45}N$ hole supply layer(HSL) (p-type concentration of 1×10^{18} cm^{-3}) and 100 nm-thick Mg-doped GaN layer((p-type concentration of 3×10^{18} cm^{-3}) along [0001] orientation. The active region consists of five 2 nm-thick $Al_{0.45}Ga_{0.55}N$ quantum wells sandwiched between six 10 nm-thick $Al_{0.55}Ga_{0.45}N$ barriers, see the purple area in Figure 1. To improve the performance of DUV LED, other three structures with different $Al_xGa_{1-x}N$ linear descending layers(denoted as S1, S2 and S3) have been designed. S1 is same as S0 except for HSL, which is 10 nm-thick Mg-doped $Al_xGa_{1-x}N$ (x value decreases linearly from 0.6 to 0.45, and p-type concentration of 1×10^{18} cm^{-3}), see the red curve in Figure 1. S2 differs from S1 only in five barriers of the active region, the first quantum barrier (QB1) is a 10nm-thick $Al_{0.558}Ga_{0.442}N$ barrier, the following four QBs with continuously decreased Al composition (QB2: $Al_{0.558\to0.556}Ga_{0.442\to0.444}N$, QB3: $Al_{0.556\to0.554}Ga_{0.444\to0.446}N$, QB4: $Al_{0.554\to0.552}Ga_{0.446\to0.448}N$, QB5: $Al_{0.552\to0.55}Ga_{0.448\to0.45}N$) to replace the traditional flat QBs, the last QB6 is 10 nm-thick $Al_{0.55}Ga_{0.45}N$ barrier near the EBL. S3 is the same as S2 except for the optimized n-type layer (NTL) that contains 5 nm p-$Al_xGa_{1-x}N$ (x value decreases linearly from 0.55 to 0.5, and p-type concentration is 1×10^{18} cm^{-3}.) and 5 nm p-$Al_{0.5}Ga_{0.5}N$ layer, see the purple curve in Figure 1.

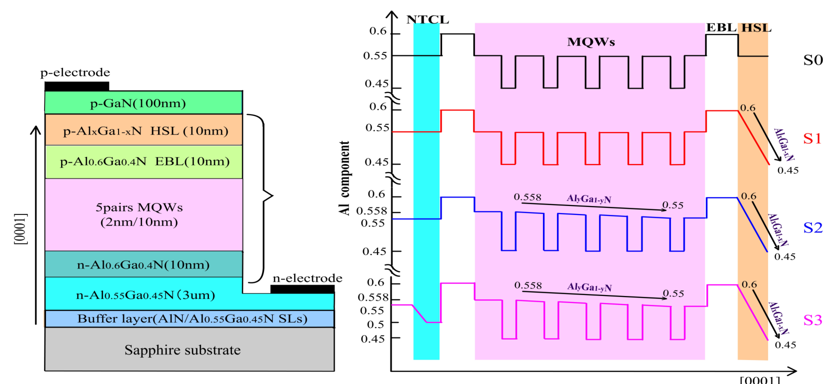

Figure 1. Structural diagrams of four DUV LEDs.

For the $Al_xGa_{1-x}N$ linear descending layer, the bandgap of $Al_xGa_{1-x}N$ material is estimated from the Vergard's law [28]:

$$E_g = x \cdot E_g^{AlN} + (1-x) \cdot E_g^{GaN} - b \cdot x \cdot (1-x). \quad (1)$$

Where, the bowing parameter b is 0.94eV. Usually, the band gap of GaN is 3.4 eV and that of AlN is 6.2 eV.

The EQE(external quantum efficiency) of LED is determined by IQE and light extraction efficiency (LEE), which can be calculated by measuring the light output power (LOP). Where η_j and η_r represent of the current injection efficiency and radiative recombination efficiency, respectively. EQE and LOP are estimated by using the following equations [29–32]:

$$EQE = IQE \cdot LEE = \eta_r \cdot \eta_j \cdot LEE = \frac{Bn^2}{An + Bn^2 + Cn^3} \cdot \eta_j \cdot LEE, \quad (2)$$

$$LOP = EQE \cdot I \cdot \frac{hc}{e\lambda}, \quad (3)$$

where n is the electron concentration. I, h, c and λ are the forward current, Planck constant, velocity of light and peak wavelength, respectively. A, B and C are the SRH recombination coefficient, respectively. The radiative recombination coefficient and auger recombination coefficient, respectively. The radiative recombination rate R_{sp} of LED is closely related to the carrier concentrations and is given as [33]:

$$R_{sp} = B(np - n_0 p_0) = B(np - n_i^2). \quad (4)$$

Here, p and n_i are the hole concentration and intrinsic carrier concentration, respectively. n_0 and p_0 are electron concentration and hole concentration in thermal equilibrium, respectively.

The photoelectric performance of LED is carried out by using the advanced physical model of semiconductor device software (APSYS) of Crosslight Software Inc, a well-known photoelectric characteristics calculated software and has been widely used in the research and analysis of semiconductor device [34,35]. The operating temperature, SRH recombination life, auger recombination and background loss are set to be 300 K, 5 ns, 1×10^{-30} cm^6/s and 2000 m^{-1}, respectively. The band-offset value is 0.75, the polarization charge is set to be 40%, the other physical parameters used in this calculation can be found in the references [6,33,35–37]. The emission spectrums, light output powers and IQEs of four DUV LEDs are calculated in this work.

3. Results and Discussion

Figure 2 shows that the IQEs and the LOPs of DUV LEDs under different injection current. It can be observed clearly from Figure 2a that the LOPs of four DUV LEDs increase with the increase of injection current. At 200 mA, S3 has the maximum LOP of 57.1 W among four DUV LEDs, while the LOPs of S0, S1 and S2 are 22.9 mW, 31.8 mW and 46.2 mW, respectively. The LOP of S3 is more than twice as that of S0 at 200 mA. As can be seen from Figure 2b that the maximum IQEs of S0, S1, S2 and S3 are 28.9%, 38.5%, 57.1% and 70.1%, respectively. Efficiency droop (abbreviated as ED) is an important index to evaluate the performance stability of LED, which is defined as ED=(IQE_{max}-IQE_{200mA})/ IQE_{max}. The EDs of S0, S1, S2 and S3 are 7%, 4.3%, 5.49% and 4.7%, respectively. Obviously, the stability of S1, S2 and S3 are better than S0. To explain the reason of performance improvement, the energy band diagram, carrier concentration, electronstatic field and radiative recombination rate are analyzed.

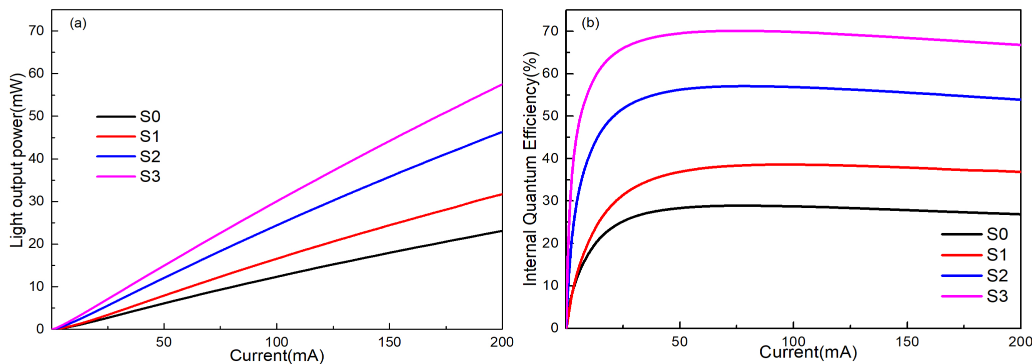

Figure 2. (**a**) Light output powers, (**b**) internal quantum efficiencies of four DUV LEDs.

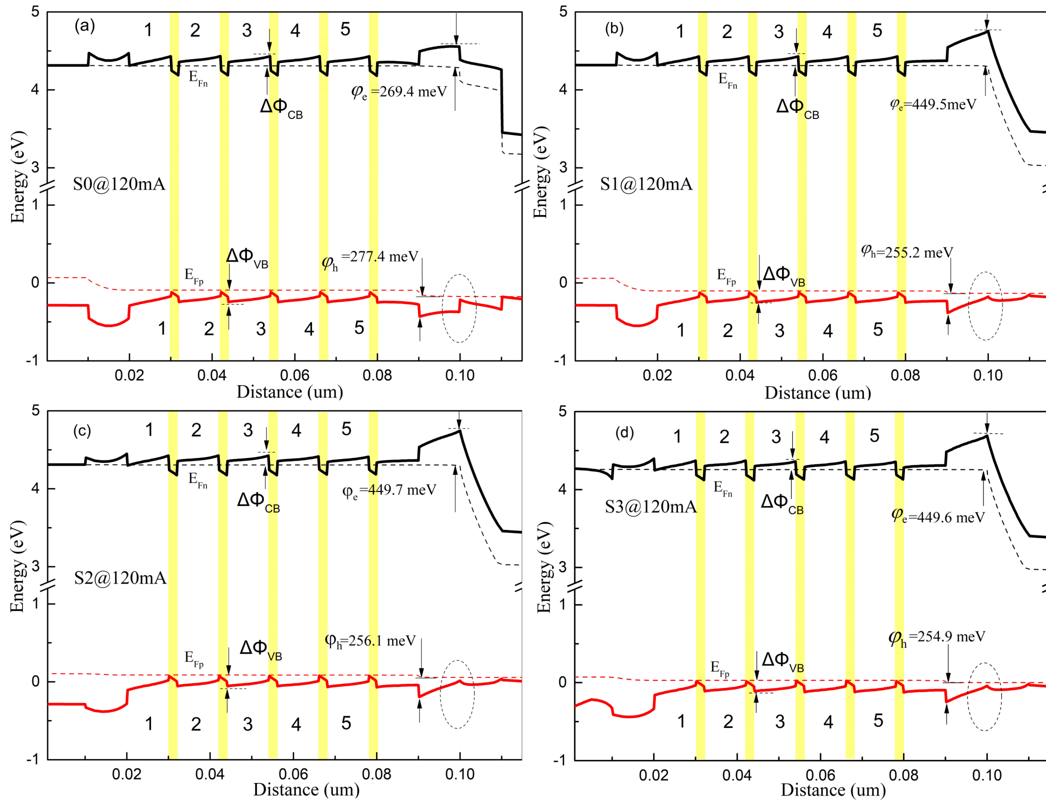

Figure 3. Energy band diagrams of four UV LEDs at 120 mA.

Figure 3 shows the energy band diagrams of four LEDs at 120 mA.The electron effective barrier height (φ_e) and the hole effective barrier height(φ_h) of EBL are marked in Figure 3. It can be observed from Figure 3a that the φ_e and φ_h of S0 are 269.4 meV and 277.4 meV respectively, while the φ_e and φ_h of S1 are 449.5 meV and 255.2 meV respectively (in Figure 3b). The φ_e and φ_h of S2 are 449.7 meV and 256.1 meV, closing to those of S1. Figure 3d shows that the φ_e and φ_h of S3 are 449.6 meV and 254.9 meV. It's well-known that electrons need to overcome conductor band barrier to leak into the p-region, and hole need to overcome valence band barrier and inject into the active region. The φ_e of S1, S2 and S3 are higher than that of S0, which means that less electrons of S1,S2 and S3 can be leaked through the EBL to the p-type region. Besides, the φ_h of S1, S2 and S3 are lower than that of S0, meanwhile the valance band of S0 has an obvious step (see the circled areas of Figure 3), these convince that the holes of S1, S2 and S3 are easier to pass through the EBL and recombine with electrons compared with S0.

To evaluate the impact of linear Al-composition graded (LACG) QB on the active region, the energy barrier height for electrons ($\Delta\Phi_{CB}$) was defined as the energy difference between E_{Fn} and the highest point of the conduction band in each QB. The energy barrier height for holes ($\Delta\Phi_{VB}$) was defined as the energy difference between E_{Fp} and the lowest point of the valence band in each QB. The average values of $\Delta\Phi_{CB}$ and $\Delta\Phi_{VB}$ of five QBs are listed in Table 1. As can be seen from Table 1, the average electron effective barrier height of S0, S1, S2 and S3 decreases gradually, which is similar to the average hole effective barrier height of S0, S1, S2 and S3. Because the lower effective barrier height facilitates the migration of carriers, and considering with the above analysis of φ_e and φ_h, so more electrons and holes will flow into MQWs of S3, better than those of S0, S1 and S2.

Table 1. The average $\Delta\Phi_{CB}$ and $\Delta\Phi_{VB}$ in five QBs of four DUV LEDs.

	S0	S1	S2	S3
$\Delta\Phi_{CB}$ (meV)	115.6	115.4	112.3	112.1
$\Delta\Phi_{VB}$ (meV)	153.5	153.2	142.7	142.5

To clearly understand the difference of carrier concentration in the active regions of different LEDs, the electron concentrations and hole concentrations in the active regions of four DUV LEDs at 120 mA are given in Figure 4. As can be seen in Figure 4 that the differences on the carrier concentrations of S0, S1, S2 and S3 are obvious. The integrated electron concentrations of S0, S1, S2 and S3 in five QWs are 0.977×10^{14} cm^{-2}, 1.129×10^{14} cm^{-2}, 1.311×10^{14} cm^{-2}, 1.546×10^{14} cm^{-2}, respectively. The integrated hole concentrations of S0, S1, S2 and S3 are 0.917×10^{14} cm^{-2}, 1.087×10^{14} cm^{-2}, 1.291×10^{14} cm^{-2} and 1.479×10^{14} cm^{-2}, respectively. Hence S3 have the largest carrier concentrations among the four DUV LEDs. The results of carrier concentrations in Figure 4 are consistent with the above analysis of the effective barrier height in Figure 3 and the average barrier height in Table 1.

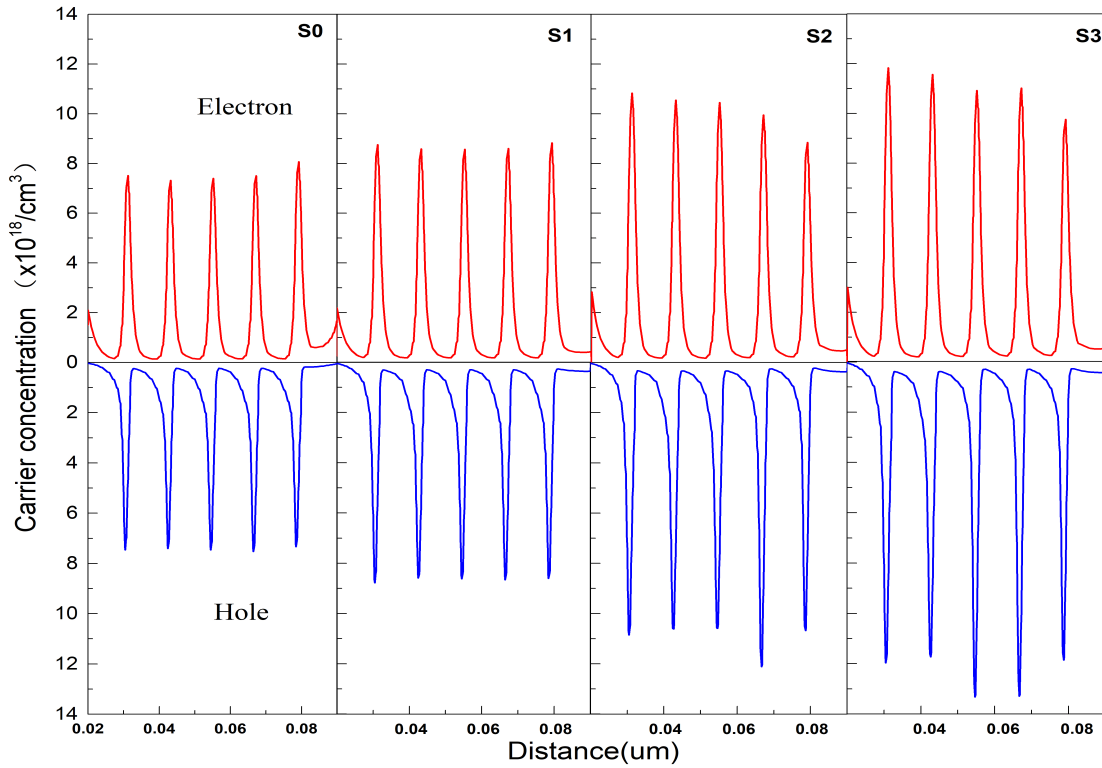

Figure 4. Carrier concentrations in the active region of four DUV LEDs at 120mA.

Figure 5a shows that S3 has an obvious electron concentration peak called two-dimensional electron gas (2DEG) [38] at 0.01 μm, where is the interface between NTL and $Al_{0.6}Ga_{0.4}N$ layer, but S0, S1 and S2 have no accumulation of electron concentration around the interface, so the exist of 2DEG can induce more electron to stored at the interface and enhance injection probability. Besides, It can be observed that the electron leakage of S0 is the most obvious among four DUV LEDs in Figure 5a. Figure 5b shows the differences of the hole concentrations of S1,S2 and S3 are very small in EBL due to the minor difference of $\Delta\Phi_{VB}$ as shown in Figure 3.

The structure design of LED not only changes the concentration of carriers in the MQWs, but also influences the electrostatic field distribution. In the AlGaN DUV LEDs, the total polarization induced charge density (Δp_{tot}) results from piezoelectric polarization induced charge density (p_{pz}) and spontaneous polarization induced charge density (p_{sp}) ,the electronstatic field in QWs (E_w) has a relationship with Δp_{tot}, and they are defined by following equations [12,39]:

$$E_w \approx \frac{l_b \cdot \Delta p_{tot}}{l_b \cdot \varepsilon_w + l_w \cdot \varepsilon_b}, \tag{5}$$

where l_b and l_w are the thicknesses of QB and QW, respectively. According the Eq.(5), the lower Δp_{tot} means weaker E_w in the active region. Besides, the QCSE is reduced and the overlap of electron-hole wavefunction ($\Gamma_{e\text{-}h}$) will increase as the electronstatic field decreases [6,40].

The migration velocity(V) of electrons is related to the kinetic energy (E_k) and the electronstatic field (E),

them are expressed as $V=\mu_e E$, $E_k=m_e^* v^2/2$ [41],where μ_e is the electron mobility and m_e^* is the electron effective mass. Figure 5c shows that S3 has the highest negative electronstatic field near the interface between NTL and $Al_{0.6}Ga_{0.4}N$ layer. Higher electronstatic field increases the velocity of electron and makes more electrons flow into the active region for S3 compared to other LEDs.The inset of Figure 5c shows that the electronstatic field in the MQWs of S1,S2 and S3 are lower than that of S0, which indicates the better overlap of $\Gamma_{e\text{-}h}$ in S1, S2 and S3 compared to S0, which is clearly shown in the Figure 5d (only the third QW is shown).

To better explain the increasing carrier concentration in the optimized HSL. the schematic diagram of charge and hole migration in p-$Al_xGa_{1\text{-}x}N$ HSL is given in Figure 6, and take the Ga-polar material based on the [0001] orientation sapphire substrate using MOCVD growth technology [42]. For the p-$Al_xGa_{1\text{-}x}N$ HSL of S1, S2 and S3, many negative polarization charges locate at the infinite number of contiguous $Al_xGa_{1\text{-}x}N$/ $Al_yGa_{1\text{-}y}N(x>y)$ interface [43], which attracts more holes move toward the active region through the p-$Al_xGa_{1\text{-}x}N$ HSL and EBL, the amount of hole injection will be increased greatly, and this phenomenon is called as three-dimensional hole gas(3DHG) [7,44–47]. In a word, the p-$Al_xGa_{1\text{-}x}N$ HSL helps more holes accelerate to the active region through EBL, therefore the hole concentrations of S1,S2 and S3 are obvious higher than that of S0,which is in agreement of the analysis in Figure 4.

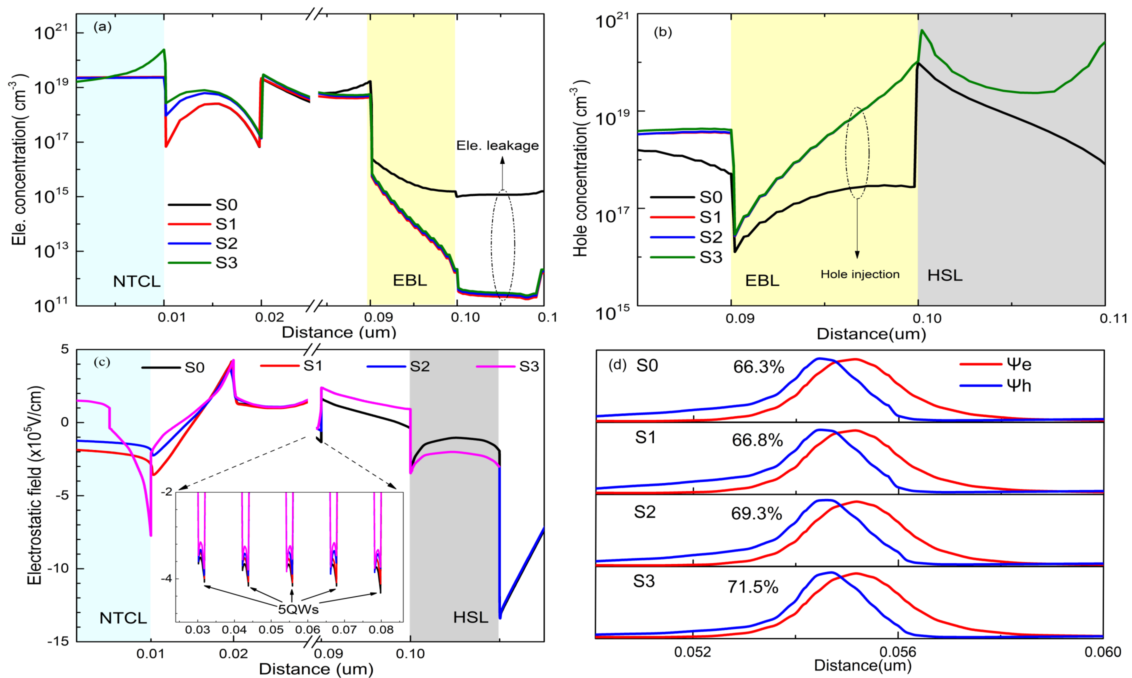

Figure 5. (**a**) Electron concentrations around NTL and EBL, (**b**) hole concentrations around EBL and HSL. (c) electrostatic fields of four LEDs at 120mA (the inset is an enlarged view of the electronstatic field in five MQWs), (d) the overlap of electron-hole's wavefunction in the third quantum well at 120mA.

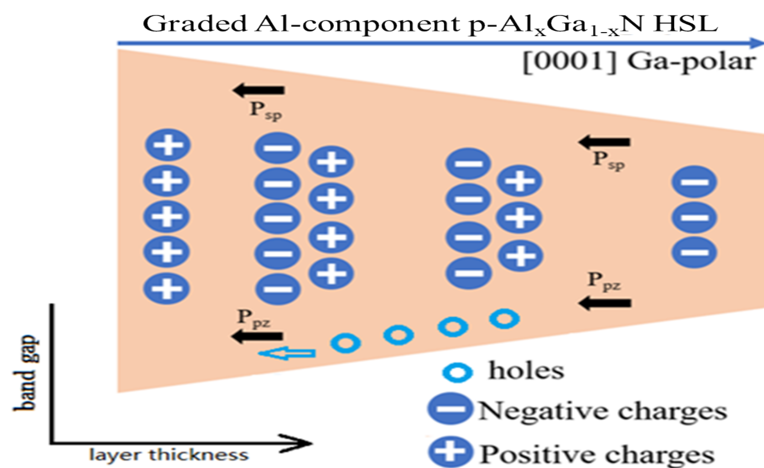

Figure 6. Schematic diagram of charge and hole migration in p-$Al_xGa_{1\text{-}x}N$ HSL.

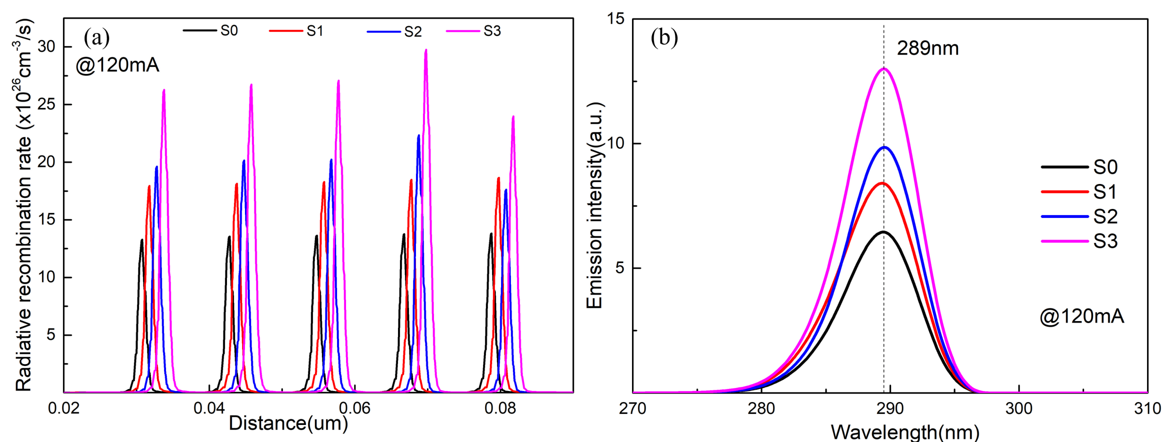

Figure 7. (**a**) Radiative recombination rates, (**b**) emission spectrums at 120mA for different LEDs**.**

To analyze the emission properties of different LEDs, Figure 7 shows the radiative recombination rates and the emission spectrums of four DUV LEDs at 120mA. The horizontal positions in Figure 7a of S1, S2 and S3 are shifted slightly for easy comparison. It's clearly observed in Figure 7a that the radiative recombination rates of S1, S2 and S3 are higher than S0.Higher radiative recombination is results from the higher overlap rate of Γ_{e-h} as well as higher carrier concentration. Compared to S0, the overlap rates in Figure 5d and carrier concentrations in Figure 4 of S1, S2 and S3 are obvoius better. Hence S1, S2 and S3 have the higher radiative recombination rate in the MQWs than S0, and the radiative recombination rate of S3 is the best among four LEDs. As can be seen in Figure 7b that the spectral intensities of S0, S1, S2 and S3 increase gradually and S3 has the highest emission intensity. Meanwhile, the peak wavelength of S3 is about 289 nm, which is same to other three DUV LEDs. As a whole, the enhanced performance of S1, S2 and S3 should attribute to the $Al_xGa_{1-x}N$ linear descending layers, the optimized NTL favors more electrons to be injected to the active region, the LACG QBs increase the overlap of electron-hole wavefunction in the MQWs, the LACG HSL can increase the hole concentration and assist EBL to reduce electron leakage simultaneously. Under the help of three optimized structures, S3 has the best emission characteristics.

4. Conclusion

In summary, four AlGaN-based DUV LEDs have been investigated numerically by replacing the traditional structure with the $Al_xGa_{1-x}N$ linear descending layers, including the optimized NTL, LACG QBs and HSL, which can effectively increase the electron and hole concentrations in the MQWs, and improve the radiative recombination rates. S3 has the best IQE and the highest light output power. Therefore, the AlGaN-based DUV LED with $Al_xGa_{1-x}N$ linear descending layers would provide a potential way to develop a high-efficiency DUV LED.

Funding

Not applicable.

Author Contributions

Conceptualization, X.C. and H.Z.; writ-ing—original draft preparation and writing—review and editing, X.C. and H.Z. All of the authors read and agreed to the published the final manuscript.

Institutional Review Board Statement

Not applicable.

Informed Consent Statement

Not applicable.

Data Availability Statement

Not applicable.

Conflicts of Interest

The authors declare no conflict of interest.

References

1 Muhammad U, Malik S, Khan MA, Hirayama H. Suppressing the Efficiency Droop in the AlGaN–Based UVB LED. *Nanotechnology* 2021; **32**(**21**): 215703.

2 Inagaki H, Saito A, Sugiyama H, Okabayashi T, Fujimoto S. Rapid Inactivation of SARS–CoV–2 with Deep –UV LED Irradiation. *Emerging Microbes & Infections* 2020; **9**(**1**): 1744–1747.

3 Ren Z *et al*. Band Engineering of III–Nitride–Based Deep–Ultraviolet Light–Emitting Diodes: a Review. *Journal of Physics D: Applied Physics* 2019; **53**(**7**): 073002.

4 X Deng, L Li, M Enomoto, Y Kawano. Continuously Frequency–Tuneable Plasmonic Structures for Terahertz Bio–Sensing and Spectroscopy. *Scientific Reports* 2019; **9**(**1**): 498.

5 M Kneissl, T–Y Seong, J Han, H Amano. The Emergence and Prospects of Deep–Ultraviolet Light–Emitting Diode Technologies. *Nature Photonics* 2019; **13**(**4**): 233–244.

6 H Yu *et al*. Advantages of AlGaN–Based Deep–Ultraviolet Light–Emitting Diodes with an Al–Composition Graded Quantum Barrier. *Optics Express* 2019; **27**(**20**): A1544–A1553.

7 Liu Z, Yu H, Ren Z, Dai J, Chen C, Sun H. Polarization–Engineered AlGaN Last Quantum Barrier for Efficient Deep–Ultraviolet Light–Emitting Diodes. *Semiconductor Science and Technology* 2020; **35**(**7**): 075021.

8 Hao G–D, Taniguchi M, Inoue S–I. Enhancement of Current Injection Efficiency of AlGaN–Based Deep–Ultraviolet Light–Emitting Diodes by Controlling Strain Relaxation. *Journal of Physics D: Applied Physics* 2020; **53**(**50**): 505107.

9 Gu W *et al*. BAlN for III–Nitride UV Light–Emitting Diodes: Undoped Electron Blocking Layer. *Journal of Physics D: Applied Physics* 2021; **54**(**17**): 175104.

10 Mondal RK, Chatterjee V, Prasad S, Pal S. Suppression of Efficiency Droop in AlGaN Based Deep UV LEDs Using Double Side Graded Electron Blocking Layer. *Semiconductor Science and Technology* 2020; **35** (**5**): 055031.

11 Wang L, He W, Zheng T, Chen Z, Zheng S. Enhanced Optical Performance of AlGaN–Based Deep–Ultraviolet Light–Emitting Diode with M–Shaped Hole Blocking Layer and W–Shaped Electron Blocking Layer. *Superlattices and Microstructures* 2019; **133**: 106188.

12 Sharif MN, Niass MI, Liou JJ, Wang F, Liu Y. p–AlInN Electron Blocking Layer for AlGaN–Based Deep–Ultraviolet Light–Emitting Diode. *Superlattices and Microstructures* 2021; **158**: 107022.

13 Deng X, Oda S, Kawano Y. Frequency Selective, High Transmission Spiral Terahertz Plasmonic Antennas. *Journal of Modeling and Simulation of Antennas and Propagation* 2016; **2**: 1–6.

14 Deng X, Kawano Y. Surface Plasmon Polariton Graphene Midinfrared Photodetector with Multifrequency Resonance. *Journal of Nanophotonics* 2018; **12**(**2**): 026017–026017.

15 Wang Y *et al*. Deep Ultraviolet Light Source from Ultrathin GaN/AlN MQW Structures with Output Power over 2 Watt. *Advanced Optical Materials* 2019; **7**(**10**): 1801763.

16 Lu Y *et al*. Carrier Manipulation and Performance Enhancement of N–polar AlGaN–based LED with Grading Quantum Barriers. *Acta Photonica Sinica* 2019; **48**(**7**): 723001.

17 Xing C *et al*. Performance Improvement of AlGaN–Based Deep Ultraviolet Light–Emitting Diodes with Step–Like Quantum Barriers. *IEEE Journal of Quantum Electronics* 2019; **56**(**1**): 1–6.

18 Bui HQT *et al*. Enhancing Efficiency of AlGaN Ultraviolet-B Light-Emitting Diodes with Graded p-AlGaN Hole Injection Layer. *Physica Status Solidi (A)* 2021; **218**(**15**): 2100003.

19 Liu N, Gu H, Wei Y, Zheng S. Performance Enhancement of AlGaN–Based Deep Ultraviolet Light–

Emitting Diodes by Using Stepped and Super – Lattice N – Type Confinement Layer. *Superlattices and Microstructures* 2020; **141**: 106492.

20 Li L, Miyachi Y, Miyoshi M, Egawa T. Enhanced Emission Efficiency of Deep Ultraviolet Light–Emitting AlGaN Multiple Quantum Wells Grown on an N–AlGaN Underlying Layer. *IEEE Photonics Journal* 2016; **8**(**5**): 1–10.

21 Gupta H *et al*. Improvement in Efficiency and Luminous Power of AlGaN–Based D–UV LEDs by Using Partially Graded Quantum Barriers. *Superlattices and Microstructures* 2020; **142**: 106543.

22 Yu H *et al*. Enhanced Performance of an AlGaN–Based Deep–Ultraviolet LED Having Graded Quantum Well Structure. *IEEE Photonics Journal* 2019; **11**(**4**): 1–6.

23 Liu Y, Yang H, Wu C. Unveiling Patterns: A Study on Semi – Supervised Classification of Strip Surface Defects. *IEEE Access* 2023; **11**: 119933–119946.

24 Zhou L, Luo Z, Pan X. Machine Learning – Based System Reliability Analysis with Gaussian Process Regression. 2024. arXiv:2403.11125.

25 Zhao Y, Dai W, Wang Z, Ragab AE. Application of Computer Simulation to Model Transient Vibration Responses of GPLs Reinforced Doubly Curved Concrete Panel Under Instantaneous Heating. *Materials Today Communications* 2024; **38**: 107949.

26 Chu C *et al*. On the Impact of Electron Leakage on the Efficiency Droop for AlGaN Based Deep Ultraviolet Light Emitting Diodes. *IEEE Photonics Journal* 2020; **12**(**3**): 1–7.

27 Sugaya T, Deng X. Resonant Frequency Tuning of Terahertz Plasmonic Structures Based on Solid Immersion Method. In Proceedings of the 2019 44th International Conference on Infrared, Millimeter, and Terahertz Waves (IRMMW–THz), Paris, France, 1–6 September 2019.

28 Coughlan C, Schulz S, Caro MA, O'Reilly EP. Band Gap Bowing and Optical Polarization Switching in Al Ga N Alloys. *Physica Status Solidi (B)* 2015; **252**(**5**): 879–884.

29 Chang J-Y, Chang H-T, Shih Y-H, Chen F – M, Huang M – F, Kuo Y – K. Efficient Carrier Confinement in Deep–Ultraviolet Light–Emitting Diodes with Composition–Graded Configuration. *IEEE Transactions on Electron Devices* 2017; **64**(**12**): 4980–4984.

30 Hirayama H. Recent progress in AlGaN deep – UV LEDs. In *Light – Emitting Diode: An Outlook on the Empirical Features and Its Recent Technological Advancements*; IntechOpen: London, UK, 2018.

31 Choi Y-H, Ryu G-H, Ryu H-Y. Evaluation of the Temperature–Dependent Internal Quantum Efficiency and the Light – Extraction Efficiency in a GaN – Based Blue Light – Emitting Diode by Using a Rate Equation Model. *Journal of the Korean Physical Society* 2016; **69**: 1286–1289.

32 Wang L *et al*. Evaluation of Internal Quantum Efficiency of Blue Light Emitting–Diodes. *Scientia Sinica Physica Mechanica & Astronomica* 2015; **45**(**6**): 067304.

33 Piprek J. *Semiconductor Optoelectronic Devices: Introduction to Physics and Simulation*; Academic press: Cambridge, MA, USA, 2003.

34 APSYS by Crosslight Software Inc., Burnaby, Canada. Available online: https://crosslight. com/products/ apsys/(accessed 2 January 2024).

35 Guttmann M *et al*. Optical Light Polarization and Light Extraction Efficiency of AlGaN – Based LEDs Emitting Between 264 and 220 nm. *Japanese Journal of Applied Physics* 2019; **58**(**SC**): SCCB20.

36 He L *et al*. Marked Enhancement in the Efficiency of Deep Ultraviolet Light–Emitting Diodes by Using a AlxGa1–XN Carrier Reservoir Layer. *Applied Physics Express* 2019; **12**(**6**): 062013.

37 Guo Y, Yan J, Zhang Y, Wang J, Li J. Enhancing the Light Extraction of AlGaN–Based Ultraviolet Light–Emitting Diodes in the Nanoscale. *Journal of Nanophotonics* 2018; **12**(**4**): 043510–043510.

38 Al Mustafa N *et al*. The Coexistence of Two – Dimensional Electron and Hole Gases in GaN – Based Heterostructures. *Journal of Applied Physics* 2012; **111**(**4**): 044512.

39 Zhang Z–H *et al*. Self–Screening of the Quantum Confined Stark Effect by the Polarization Induced Bulk Charges in the Quantum Barriers. *Applied Physics Letters* 2014; **104**(**24**): 243501–243501-5.

40 Ren Z *et al*. III–Nitride Deep UV LED Without Electron Blocking Layer. *IEEE Photonics Journal* 2019; **11** (**2**): 1–11.

41 Zhang Z – H, Zhang Y, Sun XW, Bi W. Hole Accelerator for III – Nitride Light – Emitting Diodes. In *Handbook of Solid–State Lighting and LEDs*; CRC Press: Boca Raton, FL, USA, 2017.

42 Ambacher O *et al*. Two – Dimensional Electron Gases Induced by Spontaneous and Piezoelectric Polarization Charges in N–and Ga–Face AlGaN/GaN Heterostructures. *Journal of Applied Physics* 1999; **85** (**6**): 3222–3233.

43 Wu J, Li P, Zhou X, Wu J, Hao Y. Increasing the Carrier Injection Efficiency of Gan–Based Ultraviolet Light – Emitting Diodes by Double Al Composition Gradient Last Quantum Barrier and P – Type Hole Supply Layer. *IEEE Photonics Journal* 2021; **13**(**2**): 1–8.

44 Shur M, Bykhovski A, Gaska R, Yang J, Simin G, Khan M. Accumulation Hole Layer in P – GaN/AlGaN Heterostructures. *Applied Physics Letters* 2000; **76**(**21**): 3061–3063.

45 Zhang Z–H *et al*. p–Doping–Free InGaN/GaN Light–Emitting Diode Driven by Three–Dimensional Hole Gas. *Applied Physics Letters* 2013; **103**(**26**): 263501–263501-5.

46 Zhang Z–H *et al*. Increasing the Hole Energy by Grading the Alloy Composition of the P – Type Electron Blocking Layer for Very High–Performance Deep Ultraviolet Light–Emitting Diodes. *Photonics Research* 2019; **7**(**4**): B1–B6.

47 Zhang Y *et al*. Design of P – Type Cladding Layers for Tunnel – Injected UV – A Light Emitting Diodes. *Applied Physics Letters* 2016; **109**(**19**): 191105.

© The Author(s) 2023. Published by Global Science Publishing (*GSP*).

This is an Open Access article distributed under the terms of the Creative Commons Attribution License (https://creativecommons.org/licenses/by/4.0), which permits unrestricted use, distribution, and reproduction in any medium, provided the original work is properly cited.